Available online at www.sciencedirect.com

ScienceDirect

IFAC Papers Online CONFERENCE PAPER ARCHIVE

IFAC PapersOnLine 56-2 (2023) 11106–11110

Plate Bending Models for Paper Manufacturing Processes and Comparisons to Simulations with Finite Element Methods

Mikko Salo, Jarno Jokinen, Matti Vilkko, Mikko Kanerva

Tampere University, Tampere, 33720 Finland (e-mail: first.last@tuni.fi).

Abstract: An analytical plate bending model is used in a novel measurement method that is being developed for feedback control of material properties in paper manufacturing. The model involves an efficient material model for paper yet allowing a selected level of material complexity. In this study, the effects of the simplifications are studied by comparing the results with a discretized model applied in finite element methods. The boundary conditions required for specifying the censoring location in the real system proves to be challenging and a specific combined load distribution might be necessary to apply the developed model.

Keywords: paper, cardboard, censor design, process control, finite element method

1. INTRODUCTION

In the field of paper machines, there are no methods for generally accepted feedback that would allow monitoring bending stiffness in-situ. This is mainly due to the lack of reliable on-line measurement systems. The control of elastic properties at the machine dry end is possible by manipulating for example web tension or moisture content Valenzuela et al. (2010).

The bending stiffness (or flexural rigidity) is an important property especially in paperboard packaging applications as it defines how much the product resists bending deformations. For example, when a weight is placed on a sheet of paper, the displacement field of the paper can be defined by its bending stiffness.

The direction, where to the dry-end web in paper manufacturing is moving during manufacturing, is called machine direction (MD). Similarly, the direction parallel to MD is cross-direction (CD). The bending stiffness can have different values in CD and MD since the paper fibers tend to align parallel to MD Niskanen (2008). Due to differences in the rates of reeling of the web, there exists tensile in-plane loads in CD and MD. Additionally, the through-thickness structure in paper is non-uniform in details.

Some on-line capable measurement systems have been studied in the past (see the works Kopkin (1999); Anttila and Pettersson (1997); Allan (2015); Valenzuela et al. (2010)). These are based on methods such as ultrasonic wave propagation in the material, rather than generating macroscopic, visually detectable deformations.

A novel method for measuring the bending stiffness and web tensile load in both CD and MD is being developed by Tampere University and an industry partner. The method applies vacuum pressure to create deformations to paper and computer imaging and photometric stereo to detect the deformations. Furthermore, a suitable material model is needed to reverse-engineer the material constants based on the known pressure difference and displacement field. A prototype of the measurement hardware has been developed by the industry partner. The method and the hardware have been tested during paper manufacturing and at a test facility to gain data for in-depth development.

The current measurement results have shown certain correlation in bending stiffness between state-of-the-art laboratory measurements and the method. However, the the results are inconsistent, noise-rich and require gain and offset with iterative values. Several attempts, to make changes in the measurement setup and hardware and some software changes, such as different filtering algorithms, have been studied with no remarkable benefit.

In this study, we conducted analyzes and discussed the analytical model with respect to well-defined simulations using finite element methods (FEM). The FEM model of paper and censor with practical settings of the measurement system was created. The displacement data from the FEM model was used as virtual paper machine (censor) input for the analytical model. The bending stiffness was solved similarly as in the real measurement prototype from data obtained by the computer imaging methods and in-line measurements of paper.

The main challenge in the analytical method is the arrangement of boundary conditions and the material model with simplifications compared to real paper. The results indicate discrepancies in stiffness output and the error depends on the load conditions. It is discussed if the boundary conditions could be implemented into the load distribution to form a 'virtual' combined load distribution.

10.1016/j.ifacol.2023.10.821

2. METHODS

In this Section, the analytical plate bending model used by the measurement method is introduced, with most details referred to via citations. The bending models are based on standard Kirchoff plate theory, and their exact formulation can be found in various solid mechanics textbooks (e.g., works Timoshenko (1959); Wang (2000); Le Van (2017)). The FEM model and simulation schema are also introduced.

2.1 Analytical plate bending models

We presume a plate that is initially flat in the xy-plane. The classical assumptions of thin plate are considered. Also, the deformation is assumed small. For material, linear-elastic regime is presumed and, hence, the axial stress components σ and strains ε are approximated by a linear relation by the elastic modulus E_{ii}. We apply Hooke's law for plate, i.e., the in-plane axial components of deformation are coupled by the Poisson's effect:

$$\begin{aligned} \varepsilon_x &= \sigma_x/E_{xx} - \nu_{xy}\sigma_y/E_{yy} \\ \varepsilon_y &= \sigma_y/E_{yy} - \nu_{yx}\sigma_x/E_{xx} \quad \text{and} \end{aligned} \tag{1}$$

Furthermore, it is presumed for simplicity that $\nu_{xy} = \nu_{yx} = \nu$. The stresses in z-direction are negligible and the second moment of area are included to the feature of 'bending stiffness' as follows:

$$D_i = \frac{E_{ii}}{1-\nu^2}\int_{-h/2}^{h/2} z^2\, dz = \frac{E_{ii}h^3}{12(1-\nu^2)}\,, \tag{2}$$

where bending stiffness in the two (main) directions can have different values.

The moments in the plate can then be calculated for conditions of small rotations, as follows:

$$\begin{aligned} M_x &= D_x\left(\frac{\partial w^2}{\partial x^2} + \nu\frac{\partial w^2}{\partial y^2}\right) \text{ and} \\ M_y &= D_y\left(\frac{\partial w^2}{\partial y^2} + \nu\frac{\partial w^2}{\partial x^2}\right), \end{aligned} \tag{3}$$

where $w(x, y)$ is the deflection (from the xy-plane) field of the middle plane of the plate. In Eq. (3), it was assumed that the angle θ_i of the deflection w in direction i is small:

$$\frac{\partial w}{\partial i} = tan(\theta_i) \approx \theta_i \ll 1.$$

With this assumption, the curvature κ_i in the direction i of the plate was approximated by

$$\kappa_i = \frac{\partial w^2}{\partial i^2}.$$

For the twisting moment, it is presumed simply that there is no coupling to axial stress components, giving, for example:

$$M_{xy} = -\int_{-h/2}^{h/2} \tau_{xy} z\, dz = \frac{E_{xy}h^3}{6}\frac{\partial w^2}{\partial x \partial y}\,. \tag{4}$$

For the case of paper model, it is considered that $\tau_{xy} = \tau_{yx}$ and, hence, $M_{xy} = -M_{yx}$. Then, keeping in mind the selection in Eq.(1), we simplify the shear effects related to twisting so that $D_{xy} = D_{yx} = D_{tw}$. These assumptions allow us to write:

$$-M_{yx} = M_{xy} = D_{tw}(1-\nu^2)\frac{\partial w^2}{\partial x \partial y}\,, \tag{5}$$

where it is also considered that $\nu_{xy} = \nu_{yx} = \nu$.

With the above fundamentals, the moment equilibrium for an elemental portion of model paper plate in this study can be concluded:

$$\begin{aligned} q = D_x&\left(\frac{\partial w^4}{\partial x^4} + \nu\frac{\partial w^4}{\partial y^2 x^2}\right) \\ &- 2D_{tw}(1-\nu^2)\frac{\partial w^4}{\partial x^2 \partial y^2} \\ &+ D_y\left(\frac{\partial w^4}{\partial y^4} + \nu\frac{\partial w^4}{\partial x^2 y^2}\right), \end{aligned} \tag{6}$$

where q is the lateral, out-of-plane load (distribution). In the following, we mark for clarity that $H = H_{c1} - 2H_{c2} = \nu(D_x + D_y) - 2 \cdot D_{tw}(1-\nu^2)$. However, this nomenclature of H should not be considered as concise material constant.

Equation (6) can be extended to a load conditions with in-plane forces N_x, N_y and N_{xy} affecting the middle plane of the plate. In such load condition, the moment equilibrium is:

$$\begin{aligned} q = D_x&\frac{\partial^4 w}{\partial x^4} + H\frac{\partial^4 w}{\partial x^2 \partial y^2} + D_y\frac{\partial^4 w}{\partial y^4} \\ &- N_x\frac{\partial^2 w}{\partial x^2} - 2N_{xy}\frac{\partial^2 w}{\partial x \partial y} - N_y\frac{\partial^2 w}{\partial y^2}. \end{aligned} \tag{7}$$

2.2 FEM-simulated plate bending

FEM is a mathematical theory for solving boundary value problems numerically. The boundary value problem exists when differential equations are solved under boundary conditions. For example, the solution of the displacement field subjected to a load is a typical practical problem. Solving the problem can be challenging analytically when complex geometries or boundary conditions exists. The FEM discretizes the problem into smaller regions, which are called elements.

Shell elements are typical structural elements, which are used when the plane-stress assumption can be made. This typically occurs when the thickness is small compared to other dimensions of the model (geometry). The main benefit of the shell element usage is the efficiency of analysis. Shell elements are usually divided into those with thin and thick shell formulation, which follow Kirchoff and first order shear deformation theory, respectively. The latter theory also takes into account the lateral (z-direction) effect of shear.

In this work, FEM analyses were performed using commercial software Abaqus by Dassault Systemes. The shell element (S4R) was chosen for the analysis. S4R is a reduced-integrated four-node general purpose element for three-dimensional space. The element provides six degrees of freedom (three translations and three rotations) at the each nodal point.

Abaqus presents the formulation of the shell element using the theorem of virtual work where the bending moment is defined as:

$$M_{\alpha\beta} = \int_h \sigma_{\alpha\beta}\bar{f}_{33}^2 S_3 dS_3 \tag{8}$$

where S_3 is the coordinate in thickness direction, $\bar{f}_{33}$ is the thickness increase factor, and h is the value of thickness.

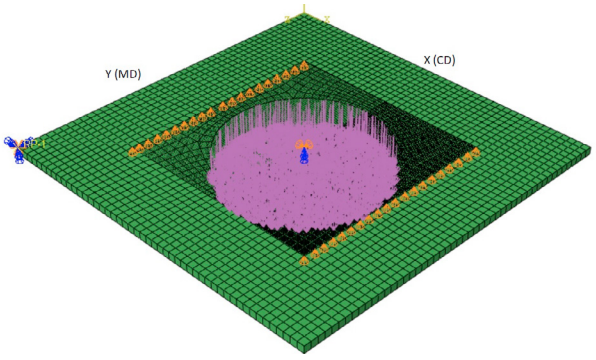

Fig. 1. An illustration of the created FEM model of the measurement system and paper. The orange cones are additional simple supports for the paper added as boundary conditions and do not represent the edges of the hole in the plate.

Stress ($\sigma_{\alpha\beta}$) is defined based on the classical constitutive relations, see Eq. (1). The shell element's bending stiffness can be derived from Eq. (8). Dassault Systemes (2021)

3. SIMULATION ARCHITECTURE

In practice, a deflection field w_p is obtained using the measurement system's prototype. The prototype consists of a metal plate with a circular hole with a diameter of 23 mm. Pressure difference ('vacuum') is generated in the hole and paper runs over this hole and experience the suction at the hole. The pressure difference, that depends on the porosity of paper, deforms the paper and is continuously measured. The deflection field $w_p(x, y)$ is then detected by means of the shape from shading using a camera and set with LED-lights. The deflection field's domain is naturally discretized by the digital camera with a resolution of 0.025 mm per pixel.

In the scope of this paper, a simulated deflection field w_f is obtained using a FEM model of the measurement setup. The FEM model was created using the version Abaqus/Standard 2021. The model is depicted in Figure 1. The three-dimensional setup included a support plate and deformable paper model. The support plate was modelled as solid, whose in-plane dimensions were 50 mm x 50 mm. The volume had a circular hole at the center (diameter 23 mm).

The deformable paper part was modelled as a plate using shell elements. The shell elements' offset was defined at the interface of the plate and paper models. The paper model's in-plane dimensions were 30 mm x 30 mm. These dimensions were chosen to exceed the hole edges. The paper thickness was 0.332 mm. The behavior of paper was modelled using linear elastic response with $E_{xx} = E_{yy} =$ 2.76 GPa and $\nu = 0.3$.

A friction-less surface to surface contact was applied between the two parts. The plate part was made rigid using a constraint. The reference point was placed at the corner of the support plate for defining the support plate's movement. All the reference point's translations and rotations were restricted. The paper part's boundary conditions were placed in the middle of the hole. In-plane translations and rotation of the paper part's normal

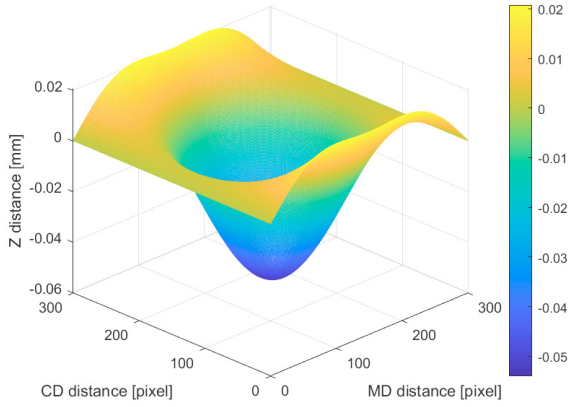

Fig. 2. The deflection field w_f generated by the FEM model. Pixel size is 0.1mm × 0.1mm.

(out-of-plane) were restricted. The model was analysed with and without out-of-plane boundary conditions at two paper edges, as shown in Fig. 1.

Pressure loading (difference) was placed in the elements locating inside the hole's region with a magnitude of -1 kPa. The geometry-defined partition was intentionally avoided because rectangular mesh for data output was needed. For that reason, the pressure loading was placed on an element-based surface and modified in the input file. The surface elements were chosen using a Matlab script that defines elements inside the specified radius. The support plate was meshed using solid elements (C3D8R) having typical in-plane dimension of 1 mm. The fine mesh was performed for the paper part. The shell element (S4R) dimension was 0.1 mm, which provides 90,000 elements in total for the paper modelling.

In the further use of FEM model output, the bending stiffnesses and tensile loads in CD and MD [1] are solved from Equation (6) or (7), depending on the case of the study, using the deflection field $w_f(x, y)$ obtained from the FEM computation (similarly to w_p obtained from a shape from shading in the practical application). A deflection field w_f corresponding the FEM setup, in Figure 1, is depicted in Figure 2. Equation (7) holds for every point (x, y) in the domain of w_f, hence a system of equations with the constant factors D_i and N_i as the unknowns is obtained. The pressure field over the measurement hole $q(x, y)$ is presumed to be the known. The system of equations is then solved using least squares and the solution gives the values of bending stiffnesses D_i and tensile loads N_i for a chosen domain Ω.

The benefit of using the FEM-simulated deflection field (w_f) compared to the real-world data (field w_p) obtained in practice is the absence of multiple error sources. In practice, errors arise, for example, from measurement device noises and inaccuracies. Also, in the case of FEM-simulated deflection, all the parameter values of the material models are known, hence comparison of values is clear.

[1] We associate the x-axis with CD and the y-axis with MD

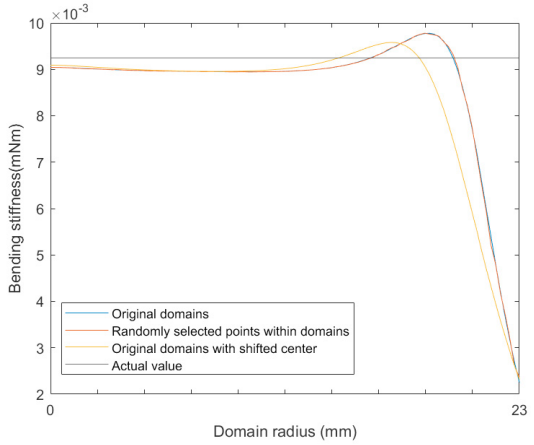

Fig. 3. Calculated bending stiffnesses and the actual one used in the model as a function of the domain size.

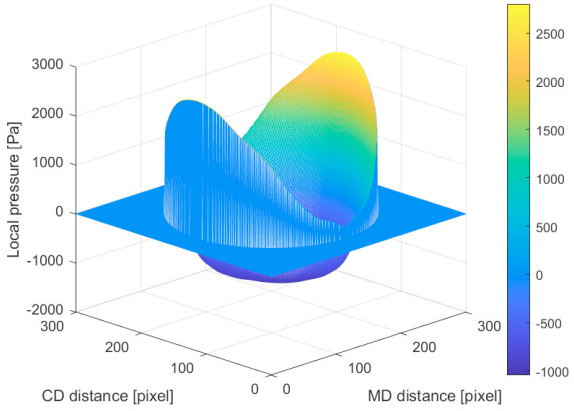

Fig. 4. The forces per unit area that complete Equation (6) for the data and parameters of FEM model. The forces are set to zero outside the area of the hole in the figure.

4. VIRTUAL TESTS AND ANALYSIS

Tests were ran using a deflection field (w_f) obtained from the FEM simulation. Here, paper was modeled isotropic with no in-plane (tensile) loads, hence one bending stiffness value (D) was solved from a system of equations (6). The domain Ω_r for x and y used to form the system of equations was a circular one with the same center as the measurement hole with a radius of r ranging from zero to 23 mm for analysis. The pressure field (q) was assumed -1 kPa within the hole and zero elsewhere. The bending stiffness solved from the system of equations for each value of r was recorded.

The first test was repeated, but in choosing the domain Ω_r of the system of equations, only random points were chosen for each r (each point had roughly a 20% chance of being picked to the domain). The first test was also repeated by moving the center of the domain by 2 mm for each r.

Tests were ran in Matlab using the same algorithm as is used in the practical prototype of the novel measurement system, whose material model is being studied. The deflection field data obtained from the FEM model was first differentiated to obtain all the partial derivatives required by Equation (7). The partial derivatives were filtered using forward and reverse digital infinite impulse response (IIR) due to significant noise especially in the higher order derivatives. The load q was set to constant, and the free parameters in Equations (6) or (7) were solved by least squares fitting with as many equations as there are points in the chosen domain Ω.

5. RESULTS AND DISCUSSION

The results of the first test are depicted in Figure 3. The results show that the correct bending stiffness can be solved at a reasonable accuracy when only using the points closer to the center of the hole as the domain. The calculated value is almost constant but has a small error compared to the real value with smaller r. With a large r, extending close to the edge of the hole, the results start changing and deviating significantly from the real (FEM input) value.

When the points are chosen randomly for each r, the results are virtually the same as when using every point. This suggest that the circular nature of Ω_r is not important, but the distance of the point from the edge of the hole. This reasoning is supported by the fact that when the center of the domain Ω_r is shifted, the results start to get deviated sooner. Here the points in the domain get closer to the edges of the hole sooner.

If the real value of D, as used in the isotropic FEM model, is plugged into Equation (6) as well as for the generated field w_f, we obtain the perfect pressure value (force per unit area, q_{ideal}). This load q_{ideal} in the area of the vacuum is depicted in Figure 4.

The ideal pressures solved are close to the actual -1 kPa near the center of the hole, but contrary to the assumed constant loads, rise to positive near the edges of the hole. The forces at the edge are not symmetric due to the asymmetric boundary conditions used in the FEM model. This would suggest that the normal forces caused by the support of the hole edges and the vacuum pressure, as well as other boundary conditions, need to be accounted for in Equation (6).

The shape of the ideal load in Figure 4 also explains that of the calculated D in Figure 3: Since q here is close to q_{ideal} near the center, Equation (6) holds for isotropic material when only one D is used to solve the system of equations described in Section 3.

When the solution of least squares problem is solved according to the analytical model (Equations (6)) with directional material (D_x, D_y and H), the solution to the isotropic FEM-simulated field should output $D_x = D_y$. However, small differences between the presumed (constant) q and q_{ideal} near the center of the hole cause the least squares solution to optimize the fit (using all the free parameters), and the actual one D is not reached. The deviation in D increases, if the system of equations is given more free parameters, according to Equation (7). In this case, there should only be one solution for D (and the in-plane loads N should become zero). This is not the case, however, for the same reasons as mentioned above.

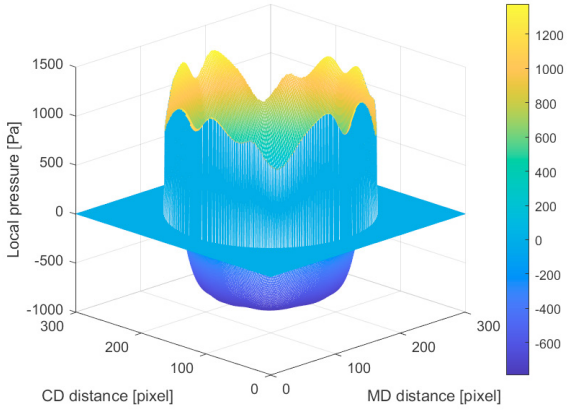

Fig. 5. Ideal load, when the simple supports parallel to MD near the hole are removed in the FEM model.

When the distributed load in the systems of equations is set to q_{ideal}, they are trivially solved for $D_x = D_y = H$ and $N_i = 0$ for any domain Ω. The ideal loading is not easy to determine though, and greatly depends on the test settings. Figure 5 depicts the same ideal load as Figure 4, but for a FEM setup where the paper part's boundary conditions are removed. The removed boundary conditions of the original FEM model are the simple supports keeping the paper part against the plate part as shown in Figure 1, parallel to MD.

The result of changing the boundary condition is apparent: as the simple support is removed, the normal forces at the edge of the hole are distributed more evenly since the paper model is more free to deform. However, now, the analytically solved load (pressure) in the middle of the hole is no longer -1 kPa. It is not currently certain whether this is an important issue to solve and how it should be accounted for in the analytical paper model. The ideal load (q), even from known ideal boundary conditions, could prove very difficult to determine so that it would result in correct material model as output of the analytical model. Also, the vacuum measurement gives only single value of pressure difference in reality.

6. CONCLUSION

This work includes the introduction to an analytical paper model to be used for a novel measurement system in paper machines. The material model used is studied using a simulated paper deformation via FEM model with known behavior. The tests run in this study show that the current model and methods used in the novel measurement system under development work in a very simple setting. The assumption of constant pressure loading q at a censor location holds true to some extent. Even small deviations in load, however, cause the model to yield inaccurate material data, especially, when more than one free parameter of bending stiffness is used. In the practical case, there exists in-plane (tensile) loads in both axial directions. Moreover, paper is not isotropic, hence a material model of six (free) parameters is to be used. Due to edge (boundary) conditions, the load q is not exactly constant and also 'virtual' q could be generated to involve realistic effects at the pressurized censor hole of measurement area.

The FEM model used in this study does not fully correspond to the real settings at paper machines. In paper machines, the loads are generated are much further away from the measurement area and the tensile in-plane loads can be much higher. There are also differences between paper machines. Although the FEM simulations here do not represent real paper machines, the assumption of a constant pressure load q does not appear to be correct in any similar test setting for use of the analytical model.

Practical measurements during paper manufacturing, at a test facility, have shown that the calculated bending stiffnesses and other material constants depend greatly on the domain of the system of equations when using certain measured displacement field and constant pressure. This should not be the case, and the results should give the correct parameter values independent of the domain used in calculating it. This variation of the solution in practice as well as the results of this study suggest that the effects of reaction forces are challenging to account for in the current procedure of using the analytical model.

The loads calculated in this study suggest that, at a minimum, the effects of reaction forces at the edges of the censor hole should be considered, as well as the effects of other boundary conditions (in-plane loading and movements of paper). Challenge about how these effects should be considered is not unambiguous. For example, in Figure 4, the loading is not that of only the pressure difference.

REFERENCES

Allan, R.J. (2015). Concepts to maximise benefit from on-line stiffness measurement. *Appita journal*, 68(3), 211–218. URL `https://search.informit.org/doi/abs/10.3316/informit.366086116725586`.

Anttila, J. and Pettersson, T. (1997). Non-contact measurement of local grammage and mechanical material properties. *Measurement science & technology*, 8(8), 921–926.

Dassault Systemes (2021). Abaqus 2021. Theory manual.

Kopkin, B. (1999). On-line measurement of strength and elastic properties of a running paper web. *Tappi journal*, 82(5), 137–140.

Le Van, A. (2017). *Nonlinear Theory of Elastic Plates*. Elsevier.

Niskanen, K. (2008). *Papermaking science and technology. Book 16, Paper Physics*. Finnish Paper Engineers' Association/Paperi ja Puu Oy.

Timoshenko, S. (1959). *Theory of plates and shells*. McGraw-Hill, New York, 2. ed. edition.

Valenzuela, M., Bentley, J., and Lorenz, R. (2010). Dynamic online sensing of sheet modulus of elasticity. *IEEE transactions on industry applications*, 46(1), 108–120. URL `https://ieeexplore.ieee.org/abstract/document/5339183`.

Wang, C.M. (2000). *Shear deformable beams and plates relationships with classical solutions*. Elsevier, Amsterdam.